A Unified Tensor-Based Joint Communication and Sensing Parameter Estimation for ISAC with Large-Scale User Access

1st Tiancheng Yang
School of Information and Electronics
Beijing Institute of Technology
Beijing, China
tiancheng_yang@bit.edu.cn

2nd Dongxuan He
School of Information and Electronics
Beijing Institute of Technology
Beijing, China
dongxuan_he@bit.edu.cn

3rd Huazhou Hou
Pervasive Communication Research Centre
Purple Mountain Laboratories
Nanjing, China
houhuazhou@pmlabs.com.cn

4th Hua Wang
School of Information and Electronics
Beijing Institute of Technology
Beijing, China
wanghua@bit.edu.cn

5th Yongming Huang
School of Information Science and Engineering
Southeast University
Nanjing, China
huangym@seu.edu.cn

6th Zhaocheng Wang
Department of Electronic Engineering
Tsinghua University
Beijing, China
zcwang@tsinghua.edu.cn

7th Tony Q.S. Quek
Information Systems Technology and Design
Singapore University of Technology and Design
Singapore
tonyquek@sutd.edu.sg

2024 IEEE International Conference on Signal, Information and Data Processing (ICSIDP) | 979-8-3315-1566-9/24/$31.00 ©2024 IEEE | DOI: 10.1109/ICSIDP62679.2024.10868366

***Abstract*—The combination of active user detection (AUD) and integrated sensing and communication (ISAC) can be utilized to realize communication and sensing functionalities over one hardware platform in the ultra-massive machine-type communications (umMTC). However, due to the received signals are typically coupled in both AUD and ISAC, it is hard to obtain the communication and sensing parameters. To solve this problem, the actual channel model is first converted into a unified form through CANDECOMP/PARAFAC decomposition (CPD) to mitigate the interference between communication and radar signals. Then, by utilizing the matrix subspace-based method, the factor matrices are accurately estimated, where the equivalent path parameters can be extracted. Furthermore, to estimate the coupled path parameters, an alternating iterative estimation algorithm is proposed. Simulation results verify the superiority of our proposed joint communication and sensing parameter estimation algorithm in AUD, channel estimation, and radar sensing.**

***Index Terms*—Active user detection, integrated sensing and communication, tensor decomposition, CPD, joint communication and sensing parameter estimation.**

I. Introduction

Active user detection (AUD) can ensure access performance for large-scale users and reduce the complexity of base station (BS) resource scheduling in grant-free random access (GF-RA) scenarios, which turns out to be a potential technology for ultra-massive machine-type communications (umMTC) application scenarios [1]. Besides, integrated sensing and communication (ISAC), which aims to achieve both communication and sensing functionalities in the same frequency band and equipment, has been proven to be a promising technology in the upcoming sixth generation (6G) networks. In particular, ISAC technology can facilitate millimeter-wave (mmWave) systems to coexist with traditional radar systems. Benefiting from the massive multiple-input multiple-output (MIMO), the significant path loss can be effectively compensated [2], thus making ISAC reliable and practical even in the mmWave band [3]. For both GF-RA and ISAC, accurate parameter estimation is the top-priority problem that needs to be solved [4]. However, it is hard to obtain the communication and sensing parameters since the received signals are typically coupled in both AUD and ISAC.

Recently, some works have been proposed to solve the parameter estimation in AUD and ISAC [5] - [7]. For AUD, channel state information (CSI) estimation and AUD are jointly realized [5] - [6]. In [5], the parameter estimation problem was transformed into a sparse signal reconstruction problem based on compressed sensing (CS), where the orthogonal matching pursuit was employed to estimate the CSI and realize the AUD. In [6], the approximate message passing algorithm was introduced in CS to improve the performance of CSI and AUD simultaneously. However, the complexity of these algorithms are typically high. For ISAC, the authors proposed a delay-Doppler-angle estimation algorithm to estimate the parameters for MIMO-ISAC systems in [7]. However, this algorithm needs the accurate communication CSI to efficiently estimate the target parameter.

The tensor theory, which is efficient to handle the high dimensional data, was introduced in signal processing [3], [8]. The authors in [3] proposed a joint tensor-based algorithm to estimate the communication and sensing parameters simultaneously in ISAC, which shows outstanding performance in estimation accuracy, sensing resolution, and training pilot overhead. In [8], the CANDECOMP/PARAFAC decomposition (CPD)-based algorithm was proposed to estimate the communication parameters according to the time domain channel matrix in a uplink system with one BS and multiple user equipments (UEs), which can save pilot overhead without performance loss. However, it is still challenging to obtain communication and sensing parameters in the scenario of large-scale user access combined with ISAC due to the coupled received signals, and the massive antenna number.

In this paper, a CPD-based joint communication and sensing parameter estimation algorithm is proposed to estimate the communication and sensing parameters for ISAC with large-scale user access. The main contributions of the paper are summarized as follows: 1) A unified CPD-based channel model for communication and sensing parameter estimation is proposed, which can effectively handle the coupled communication and

radar signals; 2) A matrix subspace-based method relying on Vandemonde structure is proposed, which can accurately estimate the factor matrices. An alternating iterative estimation algorithm consisting of two stages is proposed, which can solve the coupled parameter problem.

Notations: Scalars, vectors, matrices, and tensors are denoted by lowercase letters, lowercase boldface letters, uppercase boldface letters, and Euler script letters, respectively. The transpose, conjugate transpose, conjugate, inverse and Moore-Penrose pseudo-inverse operations are represented by $(\cdot)^T$, $(\cdot)^H$, $(\cdot)^*$, $(\cdot)^{-1}$ and $(\cdot)^\dagger$, respectively. The outer product, Kronecker product, and Khatri-Rao product are denoted by $\circ$, $\otimes$, and $\odot$, respectively. $\|\cdot\|_F$ and $\|\cdot\|_2$ are the Frobenius norm and l_2 norm, respectively. $\mathrm{Re}\{A\}$ is the real part of the complex number A, while $\mathbf{I}_N$ are the $N \times N$ identity matrix. $[\![\cdot]\!]$ is the Kruskal operator, and $\mathcal{CN}(0, \sigma^2)$ is the circularly-symmetric complex Gaussian distribution with the variance of σ^2. $diag(\mathbf{a})$ returns the diagonal matrix formed by $\mathbf{a}$. $[\mathbf{A}]_{1:m}$ and $[\mathbf{A}]_{:,m}$ are the the first m rows of $\mathbf{A}$ and the m-th column of $\mathbf{A}$, respectively. $\cap$ and $[\mathbf{A}]_c$ are the intersection and the total number of elements in set $\mathbf{A}$, respectively.

II. System Model

As shown in Fig. 1, a mmWave massive MIMO ISAC system is considered in this paper, where a full-duplex (FD) ISAC BS equipped with two antenna arrays receives the communication signals from multiple active multiple-antennas uplink UEs and uses the downlink ISAC signals to detect the point radar targets. It is assumed that N_{BS}^T antennas with M_{BS}^T radio frequency (RF) chains and N_{BS}^R antennas with M_{BS}^R RF chains are employed in the BS for transmission and reception, respectively. Without loss of generality, we assume that $N_{BS}^T = N_{BS}^R = N_{BS}$, $M_{BS}^T = M_{BS}^R = M_{BS}$, and $M_{BS} < N_{BS}$.

For the uplink communication link, U UEs equipped with N_{UE} antennas and $M_{UE} = 1$ RF chain send information to the BS, where only λU UEs are active while the remaining $(1-\lambda)U$ UEs are inactive. More specifically, we assume that $M_{UE} < N_{UE}$ and $\lambda \ll 1$. In addition, orthogonal frequency-division multiplexing (OFDM) is used to send information, where K orthogonal subcarriers are employed to send N_s independent data streams. Specifically, subcarriers $\{1, 2, ..., \overline{K}\}$ are selected as training subcarriers for parameter estimation. The u-th uplink UE sends the training communication symbol sequence $\boldsymbol{s}_u^k(n) \in \mathbb{C}^{N_S^{UE} \times 1}$ at the n-th frame and k-th subcarrier, where the corresponding training precoded communication signal $\mathbf{f}_u^k(n)$ can be expressed by

$$\mathbf{f}_u^k(n) = \mathbf{F}_{\mathrm{RF},u}^{UE} \mathbf{F}_{\mathrm{BB},u}^k(n) \boldsymbol{s}_u^k(n), \tag{1}$$

where $\mathbf{F}_{\mathrm{RF},u}^{UE} \in \mathbb{C}^{N_{UE} \times M_{UE}}$ and $\mathbf{F}_{\mathrm{BB},u}^k(n) \in \mathbb{C}^{M_{UE} \times N_S^{UE}}$ are the u-th uplink UE's analog RF precoder and digital baseband precoder at the n-th frame and the k-th subcarrier, respectively. This training precoded communication signal is processed by the analog combiner $\mathbf{W}_{\mathrm{RF}}^{\mathrm{BS}} \in \mathbb{C}^{N_{BS} \times M_{BS}}$ and digital combiner $\mathbf{W}_{\mathrm{BB}}^k \in \mathbb{C}^{M_{BS} \times N_S^{BS-R}}$ at the BS. Therefore,

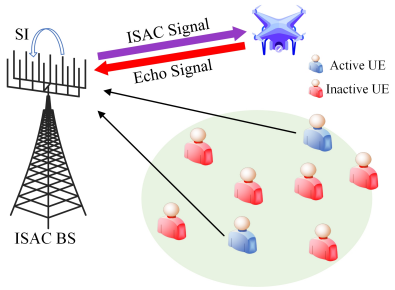

Fig. 1: System model.

the final received communication signal $\boldsymbol{y}_c^k(n) \in \mathbb{C}^{N_S^{BS-R} \times 1}$ can be presented by

$$\boldsymbol{y}_c^k(n) = \sum_{u=1}^{U} \left(\left(\mathbf{W}_{\mathrm{BB,RF}}^k \right)^H \mathbf{H}_u^k(n) \mathbf{f}_u^k(n) + \boldsymbol{n}_{\boldsymbol{c}_u}^k(n) \right), \tag{2}$$

where $\mathbf{H}_u^k(n) \in \mathbb{C}^{N_{BS} \times N_{UE}}$ is the communication channel matrix. $\mathbf{W}_{\mathrm{BB,RF}}^k = \mathbf{W}_{\mathrm{RF}}^{\mathrm{BS}} \mathbf{W}_{\mathrm{BB}}^k$ is the equivalent combiner, and $\boldsymbol{n}_{\boldsymbol{c}_u}^k(n) \in \mathbb{C}^{N_S^{BS-R} \times 1}$ is the equivalent communication noise, which is the multiplication of $\mathbf{W}_{\mathrm{BB,RF}}^k$ and the additive white Gaussian noise $\tilde{\boldsymbol{n}}_{\boldsymbol{c}_u}^k(n) \sim \mathcal{CN}(0, \sigma_c^2 \mathbf{I})$. Without loss of generality, it is assumed that $N_S^{BS-R} = M_{BS}$.

The u-th UE's frequency-domain communication channel matrix $\mathbf{H}_u(f,t)$ can be represented as

$$\mathbf{H}_u(f,t) = \sum_{l=1}^{\tilde{L}_{com}^u} \alpha_l e^{-j2\pi f \tau_l} \mathbf{a}_{\mathrm{BS}}(\theta_l) \mathbf{a}_{\mathrm{UE}}^T(\phi_l) e^{j2\pi \nu_l t}, \tag{3}$$

where $\tilde{L}_{com}^u$ denotes the total number of the u-th UE's communication paths, and α_l represents the l-th path gain. τ_l and ν_l are the delay and Doppler shift of the l-th path, respectively. $\mathbf{a}_{\mathrm{BS}}(\theta_l)$ and $\mathbf{a}_{\mathrm{UE}}(\phi_l)$ are the BS received array steering vector and UEs transmitted array steering vector, which are given by $\left[1, e^{-j2\pi \frac{d}{\lambda_c^{UE}} \sin\theta_l}, \ldots, e^{-j2\pi \frac{d(N_{BS}-1)}{\lambda_c^{UE}} \sin\theta_l}\right]^T$ and $\left[1, e^{-j2\pi \frac{d}{\lambda_c^{UE}} \sin\phi_l}, \ldots, e^{-j2\pi \frac{d(N_{UE}-1)}{\lambda_c^{UE}} \sin\phi_l}\right]^T$, respectively. ϕ_l and θ_l denote the physical real-valued angle of departure (AoD) and angle of arrival (AoA) of the l-th path, respectively. $\lambda_c^{UE} = \frac{c}{f_c^{UE}}$ represents the UEs' carrier wavelength, and f_c^{UE} is the carrier frequency. Subsequently, the communication channel $\mathbf{H}_u^k(n)$ can be obtained by discretizing continuous time series. The considered time-domain and frequency-domain scope are $t \in [nN_{all}T_s, (n+1)N_{all}T_s]$ and $f \in [-f_s/2, f_s/2]$, respectively. $N_{all}T_s = (K + N_{CP})T_s$ is the time duration of one OFDM symbol, where N_{CP} is the number of cyclic prefix in one OFDM symbol, and $f_s = \frac{1}{T_s}$ is the sampling frequency. For the time-domain sampling, the phase duration caused by Doppler shift remains constant within an OFDM symbol [9], i.e., $e^{j2\pi\nu_l t} \approx e^{j2\pi\nu_l n N_{all} T_s}$. For the frequency-domain sampling, let $f_s = \frac{kf_s}{K}$. Therefore, $\mathbf{H}_u^k(n)$ can be denoted as

$$\begin{aligned} \mathbf{H}_u^k(n) &= \mathbf{H}_u\left(\frac{kf_s}{K}, n(K+N_{CP})T_s\right) \\ &= \sum_{l=1}^{\tilde{L}_{com}^u} \alpha_l e^{-j2\pi\tau_l f_s \frac{k}{K}} \mathbf{a}_{\mathrm{BS}}(\theta_l) \mathbf{a}_{\mathrm{UE}}^T(\phi_l) \\ &\quad \times e^{j2\pi\nu_l n(K+N_{CP})T_s}, \end{aligned} \tag{4}$$

where $1 \leq k \leq \overline{K}$ and $1 \leq n \leq N$.

For the downlink ISAC link, the BS sends the OFDM-based ISAC signal to detect its surrounding targets. When the ISAC symbol sequence $\boldsymbol{s}^k(n) \in \mathbb{C}^{N_S^{BS-T} \times 1}$ is sent, the corresponding training precoded ISAC signal $\mathbf{f}_q^k(n)$ can be written by

$$\mathbf{f}_q^k(n) = \mathbf{F}_{\mathrm{RF}}^{\mathrm{BS}} \mathbf{F}_{\mathrm{BB}}^k(n) \boldsymbol{s}^k(n), \tag{5}$$

where $\mathbf{F}_{\mathrm{RF}}^{\mathrm{BS}} \in \mathbb{C}^{N_{BS} \times M_{BS}}$ and $\mathbf{F}_{\mathrm{BB}}^k(n) \in \mathbb{C}^{M_{BS} \times N_S^{BS-T}}$ are the analog RF precoder and digital baseband precoder at the BS, respectively. Once reflected by the q-th surrounding target, the final received echo signal $\boldsymbol{y}_e^k(n) \in \mathbb{C}^{M_{BS} \times 1}$ can be obtained and handled by the equivalent combiner $\mathbf{W}_{\mathrm{BB,RF}}^k$, given by

$$\boldsymbol{y}_e^k(n) = \sum_{q=1}^{Q} \big(\big(\mathbf{W}_{\mathrm{BB,RF}}^k \big)^H \mathbf{G}_q^k(n) \mathbf{f}_q^k(n) + \boldsymbol{n}_{\boldsymbol{s}_q}^{\ k}(n) \big), \tag{6}$$

where $\mathbf{G}_q^k(n) \in \mathbb{C}^{N_{BS} \times N_{BS}}$ is the sensing channel matrix, and $\boldsymbol{n}_{\boldsymbol{s}_q}^{\ k}(n) = (\mathbf{W}_{\mathrm{BB,RF}}^k)^H \tilde{\boldsymbol{n}}_{\boldsymbol{s}_q}^{\ k}(n) \in \mathbb{C}^{M_{BS} \times 1}$ is the equivalent sensing noise with $\tilde{\boldsymbol{n}}_{\boldsymbol{s}_q}^{\ k}(n) \sim \mathcal{CN}(0, \sigma_s^2 \mathbf{I})$ denoting the additive white Gaussian noise.

The q-th target's frequency-domain sensing channel matrix $\mathbf{G}_q(f,t)$ can be written as

$$\mathbf{G}_q(f,t) = \beta_q e^{-j2\pi f \tau_q} \mathbf{a}_{\mathrm{BS-R}}(\theta_q) \mathbf{a}_{\mathrm{BS-T}}^T(\phi_q) e^{j2\pi \nu_q t}, \tag{7}$$

where β_q is the q-th target's reflection coefficient, τ_q denotes the two-way time delay of the q-th target, and ν_q represents the Doppler shift of the q-th target. $\mathbf{a}_{\mathrm{BS-R}}(\theta_q)$ and $\mathbf{a}_{\mathrm{BS-T}}(\phi_q)$ are the BS received and transmitted array steering vectors, which are expressed by $\left[1, e^{-j2\pi \frac{d}{\lambda_c^{BS}} \sin\theta_q}, \ldots, e^{-j2\pi \frac{d(N_{BS}-1)}{\lambda_c^{BS}} \sin\theta_q}\right]^T$ and $\left[1, e^{-j2\pi \frac{d}{\lambda_c^{BS}} \sin\phi_q}, \ldots, e^{-j2\pi \frac{d(N_{BS}-1)}{\lambda_c^{BS}} \sin\phi_q}\right]^T$, respectively. ϕ_q and θ_q denote the AoD and AoA of the q-th target. $\lambda_c^{BS} = \frac{c}{f_c^{BS}}$ represents the BS's carrier wavelength, and f_c^{BS} is the carrier frequency. Consequently, the sensing channel $\mathbf{G}_q^k(n)$ can be given by

$$\begin{aligned} \mathbf{G}_q^k(n) &= \mathbf{G}_q\big(\frac{k f_s}{K}, n(K+N_{CP})T_s\big) \\ &= \beta_q e^{-j2\pi \tau_q f_s \frac{k}{K}} \mathbf{a}_{\mathrm{BS-R}}(\theta_q) \mathbf{a}_{\mathrm{BS-T}}^T(\phi_q) \\ &\quad \times e^{j2\pi \nu_q n(K+N_{CP})T_s}. \end{aligned} \tag{8}$$

According to (2) and (6), the ultimate signal $\boldsymbol{y}^k(n) \in \mathbb{C}^{M_{BS} \times 1}$ can be expressed by [1]

$$\boldsymbol{y}^k(n) = \boldsymbol{y}_c^k(n) + \boldsymbol{y}_e^k(n). \tag{9}$$

[1]Due to the fact that the SI signal can be suppressed by the advanced techniques, the SI is not considered in this work.

III. CPD-BASED UNIFIED MODEL FORMULATION

By substituting (2), (4), (6), and (8) into (9), the ultimate signal received by the BS can be expressed by

$$\begin{aligned} \boldsymbol{y}^k(n) = &\sum_{u=1}^{U} \big(\big(\mathbf{W}_{\mathrm{BB,RF}}^k \big)^H \big(\sum_{l=1}^{\tilde{L}_{com}^u} \alpha_l e^{-j2\pi\tau_l f_s \frac{k}{K}} \mathbf{a}_{\mathrm{BS}}(\theta_l) \\ &\times \mathbf{a}_{\mathrm{UE}}^T(\phi_l) e^{j2\pi\nu_l n(K+N_{CP})T_s} \big) \mathbf{f}_u^k(n) + \sum_{l=1}^{\tilde{L}_{com}^u} \boldsymbol{n}_{\boldsymbol{c}l}^{\ k}(n) \big) \\ &+ \sum_{q=1}^{Q} \big(\big(\mathbf{W}_{\mathrm{BB,RF}}^k \big)^H \beta_q e^{-j2\pi\tau_q f_s \frac{k}{K}} \mathbf{a}_{\mathrm{BS-R}}(\theta_q) \\ &\times \mathbf{a}_{\mathrm{BS-T}}^T(\phi_q) e^{j2\pi\nu_q n(K+N_{CP})T_s} \mathbf{f}_q^k(n) + \boldsymbol{n}_{\boldsymbol{s}_q}^{\ k}(n) \big), \end{aligned} \tag{10}$$

Subsequently, the unified form of $\boldsymbol{y}^k(n)$ can be obtained as follows

$$\begin{aligned} \boldsymbol{y}^k(n) = &\sum_{l_u=1}^{L_{com}} \big(\big(\mathbf{W}_{\mathrm{BB,RF}}^k \big)^H \alpha_{l_u} e^{-j2\pi\tau_{l_u} f_s \frac{k}{K}} \mathbf{a}_{\mathrm{BS}}(\theta_{l_u}) \\ &\times \mathbf{a}_{\mathrm{UE}}^T(\phi_{l_u}) e^{j2\pi\nu_{l_u} n(K+N_{CP})T_s} \mathbf{f}_{l_u}^k(n) + \boldsymbol{n}_{\boldsymbol{c}l_u}^{\ k}(n) \big) \\ &+ \sum_{l_q=1}^{L_{echo}} \big(\big(\mathbf{W}_{\mathrm{BB,RF}}^k \big)^H \beta_{l_q} e^{-j2\pi\tau_{l_q} f_s \frac{k}{K}} \mathbf{a}_{\mathrm{BS-R}}(\theta_{l_q}) \\ &\times \mathbf{a}_{\mathrm{BS-T}}^T(\phi_{l_q}) e^{j2\pi\nu_{l_q} n(K+N_{CP})T_s} \mathbf{f}_{l_q}^k(n) + \boldsymbol{n}_{\boldsymbol{s}l_q}^{\ k}(n) \big) \\ = &\sum_{l_a=1}^{L} \big(\big(\mathbf{W}_{\mathrm{BB,RF}}^k \big)^H \gamma_{l_a} e^{-j2\pi\tau_{l_a} f_s \frac{k}{K}} \mathbf{a}_{\mathrm{R}}(\theta_{l_a}) \mathbf{a}_{\mathrm{T}}^T(\phi_{l_a}) \\ &\times e^{j2\pi\nu_{l_a} n(K+N_{CP})T_s} \mathbf{f}_{l_a}^k(n) + \boldsymbol{n}_{l_a}^k(n) \big), \end{aligned} \tag{11}$$

where $L = L_{com} + L_{echo}$ represents the number of the entire paths, and l_a is the path index. γ_{l_a} and τ_{l_a} denote the unified path gain and time delay of the l_a-th path, respectively. $\mathbf{a}_{\mathbf{R}}(\theta_{l_a})$ and $\mathbf{a}_{\mathbf{T}}(\phi_{l_a})$ are the unified received and transmitted array steering vectors of the l_a-th path, respectively. ν_{l_a}, $\mathbf{f}_{l_a}^k(n)$, and $\boldsymbol{n}_{l_a}^k(n)$ denote the unified Doppler shift, training precoded signal, and noise of the l_a-th path, respectively. Consequently, by employing the frequency-flat beam training scheme in [2], i.e., $\mathbf{W}_{\mathrm{BB,RF}}^k = \mathbf{W}_{\mathrm{BB,RF}} = \mathbf{W}$, and $\mathbf{f}_{l_a}^k(n) = \mathbf{f}_{l_a}(n)$, the received signals $\mathbf{Y}^k$ stacking from the N frames can be written by

$$\mathbf{Y}^k = \sum_{l_a=1}^{L} e^{-j2\pi\tau_{l_a} f_s \frac{k}{K}} \tilde{\mathbf{a}}_{\mathrm{R}}(\gamma_{l_a}, \theta_{l_a}) \tilde{\mathbf{a}}_{\mathrm{T}}^T(\phi_{l_a}) \mathbf{\Gamma}(\nu_{l_a}) + \boldsymbol{N}_{l_a}^k, \tag{12}$$

where $\tilde{\mathbf{a}}_{\mathrm{R}}(\gamma_{l_a}, \theta_{l_a}) = \gamma_{l_a} \mathbf{W}^H \mathbf{a}_{\mathrm{R}}(\theta_{l_a}) \in \mathbb{C}^{M_{BS} \times 1}$ and $\tilde{\mathbf{a}}_{\mathrm{T}}(\phi_{l_a}) = \mathbf{F}_{l_a}^T \mathbf{a}_{\mathrm{T}}(\phi_{l_a}) \in \mathbb{C}^{N \times 1}$ are the equivalent received and transmitted array steering vectors of the l_a-th path, respectively, and $\mathbf{F}_{l_a} = [\mathbf{f}_{l_a}(1), \ldots, \mathbf{f}_{l_a}(N)]$ denotes the unified training precoded signal stacking from the N frames. $\mathbf{\Gamma}(\nu_{l_a}) = diag([e^{j2\pi\nu_{l_a}(K+N_{CP})T_s}, \ldots, e^{j2\pi\nu_{l_a} N(K+N_{CP})T_s}]) \in \mathbb{C}^{N \times N}$ and $\boldsymbol{N}_{l_a}^k = [\boldsymbol{n}_{l_a}^k(1), \ldots, \boldsymbol{n}_{l_a}^k(N)] \in \mathbb{C}^{M_{BS} \times N}$ denote the Doppler shift diagonal matrix and noise matrix, respectively. $\mathbf{Y}^k = [\boldsymbol{y}^k(1), \ldots, \boldsymbol{y}^k(N)] \in \mathbb{C}^{M_{BS} \times N}$ contains the entire received communication and echo signals at the k-th

subcarrier. Subsequently, the corresponding third-order tensor $\boldsymbol{\mathcal{Y}} \in \mathbb{C}^{M_{BS}\times N\times \overline{K}}$ satisfying the given CPD format [10] can be acquired by stacking the entire communication and echo signals of $\overline{K}$ training subcarriers, given by

$$\begin{aligned}\boldsymbol{\mathcal{Y}} &= [\![\mathbf{A}^{(1)}, \mathbf{A}^{(2)}, \mathbf{A}^{(3)}]\!] + \boldsymbol{\mathcal{N}} \\ &= \sum_{l_a=1}^{L} \tilde{\mathbf{a}}_{\mathrm{R}}(\gamma_{l_a}, \theta_{l_a}) \circ \tilde{\mathbf{b}}_{\mathrm{T}}(\phi_{l_a}, \nu_{l_a}) \circ \tilde{\mathbf{c}}(\tau_{l_a}) + \boldsymbol{\mathcal{N}},\end{aligned} \tag{13}$$

where $\boldsymbol{\mathcal{N}} \in \mathbb{C}^{M_{BS}\times N\times \overline{K}}$ is the unified noise tensor, and the three factor matrices $\mathbf{A}^{(1)}$, $\mathbf{A}^{(2)}$ and $\mathbf{A}^{(3)}$ can be written as

$$\mathbf{A}^{(1)} = [\tilde{\mathbf{a}}_{\mathrm{R}}(\gamma_1, \theta_1), \ldots, \tilde{\mathbf{a}}_{\mathrm{R}}(\gamma_L, \theta_L)] \in \mathbb{C}^{M_{BS}\times L}, \tag{14}$$

$$\mathbf{A}^{(2)} = [\tilde{\mathbf{b}}_{\mathrm{T}}(\phi_1, \nu_1), \ldots, \tilde{\mathbf{b}}_{\mathrm{T}}(\phi_L, \nu_L)] \in \mathbb{C}^{N\times L}, \tag{15}$$

$$\mathbf{A}^{(3)} = [\tilde{\mathbf{c}}(\tau_1), \ldots, \tilde{\mathbf{c}}(\tau_L)] \in \mathbb{C}^{\overline{K}\times L}, \tag{16}$$

where $\tilde{\mathbf{b}}_{\mathrm{T}}(\phi_{l_a}, \nu_{l_a}) = \boldsymbol{\Gamma}(\nu_{l_a})\tilde{\mathbf{a}}_{\mathrm{T}}(\phi_{l_a})$ denotes the unified transmitted array steering vector of the l_a-th path with the Doppler shift ν_{l_a}, and $\tilde{\mathbf{c}}(\tau_{l_a}) = [e^{-j2\pi\tau_{l_a} f_s \frac{k}{K}}]_{k=1}^{\overline{K}}$. It is worth noting that the objective of this paper is to estimate the unknown parameters $\{\gamma_{l_a}, \theta_{l_a}, \phi_{l_a}, \nu_{l_a}, \tau_{l_a}\}_{l_a=1}^{L}$ from $\boldsymbol{\mathcal{Y}}$, which can be mathematically expressed as

$$\underset{\mathbf{A}^{(1)},\mathbf{A}^{(2)},\mathbf{A}^{(3)}}{\text{minimize}} \left\| \boldsymbol{\mathcal{Y}} - \sum_{l_a=1}^{L} \tilde{\mathbf{a}}_{\mathrm{R}}(\gamma_{l_a}, \theta_{l_a}) \circ \tilde{\mathbf{b}}_{\mathrm{T}}(\phi_{l_a}, \nu_{l_a}) \circ \tilde{\mathbf{c}}(\tau_{l_a}) \right\|_F^2. \tag{17}$$

IV. CPD-based Unified Parameter Estimation Algorithm

A. Factor Matrices Estimation

To estimate the factor matrices of the received observation tensor $\boldsymbol{\mathcal{Y}}$, the alternating least squares (ALS)-based algorithm [12] turns to be efficient and mature. However, the structural characteristics of the factor matrix are not considered in ALS, making it fail to estimate the maximum number of path parameters from the estimated factor matrices $\{\hat{\mathbf{A}}^{(1)}, \hat{\mathbf{A}}^{(2)}, \hat{\mathbf{A}}^{(3)}\}$. To tackle this problem, a matrix subspace-based method using the Vandermonde structure characteristics of $\mathbf{A}^{(3)}$ is proposed. Specifically, considering $\mathbf{Y}_{(1)}^T = \left(\mathbf{A}^{(3)} \odot \mathbf{A}^{(2)}\right)\left(\mathbf{A}^{(1)}\right)^T + \mathbf{N}_{(1)}^T$, a cyclic selection matrix $\mathbf{J}_l = \begin{bmatrix}\mathbf{0}_{K_3\times(l-1)} & \mathbf{I}_{K_3} & \mathbf{0}_{K_3\times(L_3-l)}\end{bmatrix}$ is used to expand the dimension of $\mathbf{Y}_{(1)}$ for obtaining $\mathbf{Y}_{(1)}^e$ as follows

$$\begin{aligned}\mathbf{Y}_{(1)}^e &= \left[(\mathbf{J}_1 \otimes \mathbf{I}_N)\mathbf{Y}_{(1)}^T, \ldots, (\mathbf{J}_{L_3} \otimes \mathbf{I}_N)\mathbf{Y}_{(1)}^T\right] \\ &= \left([\mathbf{A}^{(3)}]_{1:K_3} \odot \mathbf{A}^{(2)}\right)\left([\mathbf{A}^{(3)}]_{1:L_3} \odot \mathbf{A}^{(1)}\right)^T + \mathbf{N}_{(1)}^e,\end{aligned} \tag{18}$$

where $\mathbf{N}_{(1)}^e \in \mathbb{C}^{K_3N\times L_3M_{BS}}$ is the noise matrix. Here, the last equality holds due to $\mathbf{A}^{(3)}$ has the Vandermonde structure [11]. Consequently, one can refer to [8] and use linear algebra, e.g., the truncated singular value decomposition (SVD) and the eigenvalue decomposition (EVD), to further estimate the factor matrices. Specifically, the truncated SVD is performed on $\mathbf{Y}_{(1)}^e$, and the decomposition result can be expressed as $\mathbf{Y}_{(1)}^e = \mathbf{U}\boldsymbol{\Sigma}\mathbf{V}^H$. After extracting the submatrices $\mathbf{U}_1 = [\mathbf{U}]_{1:(K_3-1)N,:} \in \mathbb{C}^{(K_3-1)N\times L}$ and $\mathbf{U}_2 = [\mathbf{U}]_{N+1:K_3N,:} \in \mathbb{C}^{(K_3-1)N\times L}$ from the left singular vector $\mathbf{U}$, the EVD can be performed to decompose the matrix $\mathbf{U}_1^\dagger\mathbf{U}_2$, given by

$$\mathbf{U}_1^\dagger\mathbf{U}_2 = \mathbf{M}\mathbf{Z}\mathbf{M}^{-1}, \tag{19}$$

where $\mathbf{M} \in \mathbb{C}^{L\times L}$ is the left eigenvector, and the diagonal matrix $\mathbf{Z} \in \mathbb{C}^{L\times L}$ contains the information of the equivalent time delays on its diagonal elements $\{z_l = e^{-j2\pi\tau_l f_s \frac{1}{K}}\}_{l=1}^{L}$. Therefore, the l_a-th column of $\hat{\mathbf{A}}^{(3)}$ can be reconstructed as

$$\hat{\mathbf{a}}_{l_a}^{(3)} = [z_{l_a}, z_{l_a}^2, \ldots, z_{l_a}^{\overline{K}}]. \tag{20}$$

Sequentially, the l_a-th column of the factor matrices $\hat{\mathbf{A}}^{(2)}$ and $\hat{\mathbf{A}}^{(1)}$ can be acquired, given by

$$\hat{\mathbf{a}}_{l_a}^{(2)} = \left(\frac{\left[\hat{\mathbf{a}}_{l_a}^{(3)}\right]_{1:K_3}^H}{K_3} \otimes \mathbf{I}_N\right)\mathbf{U}\left[\mathbf{M}\right]_{:,l_a}, \tag{21}$$

and

$$\hat{\mathbf{a}}_{l_a}^{(1)} = \left(\frac{\left[\hat{\mathbf{a}}_{l_a}^{(3)}\right]_{1:L_3}^H}{L_3} \otimes \mathbf{I}_{M_{BS}}\right)\mathbf{V}^*\boldsymbol{\Sigma}\left[\mathbf{M}^{-T}\right]_{:,l_a}, \tag{22}$$

respectively. According to (20), (21) and (22), we have

$$\hat{\mathbf{A}}^{(n)} = \mathbf{A}^{(n)}\boldsymbol{\Pi}\boldsymbol{\Delta}_n + \mathbf{E}_n, \tag{23}$$

where $n \in \{1, 2, 3\}$, and $\boldsymbol{\Pi} \in \mathbb{C}^{L\times L}$ denotes the unknown permutation matrix. $\boldsymbol{\Delta}_n$ is the unknown diagonal matrix satisfying $\boldsymbol{\Delta}_1\boldsymbol{\Delta}_2\boldsymbol{\Delta}_3 = \mathbf{I}_L$, and $\mathbf{E}_n$ represents the estimation errors of the factor matrices.

B. Path Parameters Estimation

According to (14) and (16), θ_{l_a} and τ_{l_a} can be extracted by a correlation-based scheme [2], where the estimated parameters $\hat{\theta}_{l_a}$ and $\hat{\tau}_{l_a}$ can be expressed as

$$\hat{\theta}_{l_a} = \arg\max_{\theta_{l_a}} \frac{\left|(\hat{\mathbf{a}}_{l_a}^{(1)})^H\mathbf{W}^H\mathbf{a}_{\mathrm{R}}(\theta_{l_a})\right|^2}{\left\|\hat{\mathbf{a}}_{l_a}^{(1)}\right\|_2^2\left\|\mathbf{W}^H\mathbf{a}_{\mathrm{R}}(\theta_{l_a})\right\|_2^2}, \tag{24}$$

$$\hat{\tau}_{l_a} = \arg\max_{\tau_{l_a}} \frac{\left|(\hat{\mathbf{a}}_{l_a}^{(3)})^H\tilde{\mathbf{c}}(\tau_{l_a})\right|^2}{\left\|\hat{\mathbf{a}}_{l_a}^{(3)}\right\|_2^2\left\|\tilde{\mathbf{c}}(\tau_{l_a})\right\|_2^2}, \tag{25}$$

respectively. By employing the one-dimensional search in the scope of θ_{l_a} and τ_{l_a}, respectively, the problems of (24) and (25) can be easily handled. Considering (15), the AoD and the Doppler shift are coupled, and thus the joint estimation problem of estimating ϕ_{l_a} and ν_{l_a} can be presented as

$$\hat{\mathbf{D}} = \arg\min_{\mathbf{D}} \left\|\hat{\mathbf{a}}_{l_a}^{(2)} - \delta_{l_a}\boldsymbol{\Gamma}(\nu_{l_a})\mathbf{F}_{l_a}^T\mathbf{a}_{\mathrm{T}}(\phi_{l_a})\right\|_2^2, \tag{26}$$

where $\hat{\mathbf{D}} = \{\hat{\delta}_{l_a}, \hat{\nu}_{l_a}, \hat{\mathbf{F}}_{l_a}, \hat{\phi}_{l_a}\}$ and $\mathbf{D} = \{\delta_{l_a}, \nu_{l_a}, \mathbf{F}_{l_a}, \phi_{l_a}\}$ are the estimated and true parameter sets, respectively. δ_{l_a} and $\hat{\delta}_{l_a}$ are the l_a-th true and estimated diagonal elements of $\boldsymbol{\Delta}_2$, respectively. To solve this problem, an alternating

Algorithm 1 Alternating Iterative Estimation Algorithm

Input: The estimated factor matrix $\hat{\mathbf{A}}^{(2)}$, the unified training precoded signal $\mathbf{F}_{l_a}, l_a = 1, 2, \ldots, L$ and the number of iterations N_{I}.

Output: $\{\hat{\delta}_{l_a}\}_{l_a=1}^{L}$, $\{\hat{\nu}_{l_a}\}_{l_a=1}^{L}$, and $\{\hat{\phi}_{l_a}\}_{l_a=1}^{L}$.

for $l_a = 1, 2, \ldots, L$ **do**
  Obtain the estimated training precoded signal $\hat{\mathbf{F}}_{l_a}$ and the initial value of the estimated AoD $\hat{\phi}_{l_a}^{(0)}$ according to (27).
  Let $\hat{\nu}_{l_a}^{(0)} = 0, l_a = 1, 2, \ldots, L$.
  for $i = 1, 2, \ldots, N_{\mathrm{I}}$ **do**
    Calculate $\hat{\delta}_{l_a}^{(i)}$ based on (28).
    Calculate $\hat{\nu}_{l_a}^{(i)}$ based on (29).
    Calculate $\hat{\phi}_{l_a}^{(i)}$ based on (30).
  end for
  Acquire $\hat{\delta}_{l_a} = \hat{\delta}_{l_a}^{(N_{\mathrm{I}})}$, $\hat{\nu}_{l_a} = \hat{\nu}_{l_a}^{(N_{\mathrm{I}})}$, and $\hat{\phi}_{l_a} = \hat{\phi}_{l_a}^{(N_{\mathrm{I}})}$.
end for

iterative estimation algorithm is proposed, which consists of two stages, namely, initialization stage and estimation stage. In the initialization stage, the estimated training precoded signal $\hat{\mathbf{F}}_{l_a}$ and the initial value of the estimated AoD $\hat{\phi}_{l_a}^{(0)}$ can be acquired by employing the two-dimensional search in the scope of $\mathbf{F}_{l_a}$ and ϕ_{l_a}, which can be expressed as

$$\{\hat{\mathbf{F}}_{l_a}, \hat{\phi}_{l_a}^{(0)}\} = \arg \max_{\mathbf{F}_{l_a}, \phi_{l_a}} \frac{\left|\mathbf{a}_{\mathrm{T}}^{H}(\phi_{l_a})\mathbf{F}_{l_a}^{*}\hat{\mathbf{a}}_{l_a}^{(2)}\right|^2}{\left\|\mathbf{F}_{l_a}^{T}\mathbf{a}_{\mathrm{T}}(\phi_{l_a})\right\|_2^2}. \tag{27}$$

where $\frac{\left|\mathbf{a}_{\mathrm{T}}^{H}(\phi_{l_a})\mathbf{F}_{l_a}^{*}\hat{\mathbf{a}}_{l_a}^{(2)}\right|^2}{\left\|\mathbf{F}_{l_a}^{T}\mathbf{a}_{\mathrm{T}}(\phi_{l_a})\right\|_2^2}$ is the correlation value. For inactive UEs, the order of magnitude of the correlation value is much smaller than that of active UEs and radar targets. Therefore, the total number of active UEs and radar targets can be determined by a given empirical threshold λ. Since the BS has all UEs' and targets' pilot information, it is easily to distinguish whether the current path parameter belongs to an uplink UE or a radar target. In the estimation stage, $\hat{\delta}_{l_a}$, $\hat{\nu}_{l_a}$, and $\hat{\phi}_{l_a}$ can be obtained, given by [4]

$$\hat{\delta}_{l_a}^{(i)} = \tilde{\mathbf{a}}_{\mathrm{T}}^{\dagger}(\hat{\phi}_{l_a}^{(i-1)})\hat{\mathbf{\Gamma}}^{-1}(\hat{\nu}_{l_a}^{(i-1)})\hat{\mathbf{a}}_{l_a}^{(2)}, \tag{28}$$

$$\hat{\nu}_{l_a}^{(i)} = \arg \max_{\nu_{l_a}} \sum_{n=1}^{N} \mathrm{Re}\big(e^{j2\pi\nu_{l_a} n(K+N_{CP})T_s}\hat{\delta}_{l_a}^{(i)}[\hat{\mathbf{a}}_{l_a}^{(2)}]_n^{*} \times \mathbf{f}_{l_a}^{T}(n)\mathbf{a}_T(\hat{\phi}_{l_a}^{(i-1)})\big), \tag{29}$$

$$\hat{\phi}_{l_a}^{(i)} = \arg \max_{\phi_{l_a}} \frac{\left|\mathbf{a}_{\mathrm{T}}^{H}(\phi_{l_a})\mathbf{F}_{l_a}^{*}\hat{\mathbf{\Gamma}}^{-1}(\hat{\nu}_{l_a}^{(i)})\hat{\mathbf{a}}_{l_a}^{(2)}\right|^2}{\left\|\mathbf{F}_{l_a}^{T}\mathbf{a}_{\mathrm{T}}(\phi_{l_a})\right\|_2^2}, \tag{30}$$

respectively. The details of the proposed alternating iterative estimation algorithm is summarized in Algorithm 1. After obtaining $\{\hat{\theta}_{l_a}\}_{l_a=1}^{L}$, $\{\hat{\tau}_{l_a}\}_{l_a=1}^{L}$, $\{\hat{\nu}_{l_a}\}_{l_a=1}^{L}$, and $\{\hat{\phi}_{l_a}\}_{l_a=1}^{L}$, the path gains $\{\hat{\gamma}_{l_a}\}_{l_a=1}^{L}$ can be estimated by utilizing the least-squares estimators in [4].

V. Simulation Results

In this section, simulation results are presented to verify the effectiveness of our proposed CPD-based joint communication and sensing parameter estimation. The whole number of uplink UEs is set as $U = 100$. The BS is equipped with $N_{BS} = 64$ antennas and $M_{BS} = 40$ RF chains, while the uplink UEs employ $N_{UE} = 32$ antennas with $M_{UE} = 1$ RF chain [4]. The carrier frequencies of the BS and uplink UEs are $f_c^{BS} = f_c^{UE} = 28$ GHz, and the system sampling rate is set to $f_s = 100$ MHz. The total number of frames is $N = 50$, and the total number of subcarriers is $K = 256$, where the total number of training subcarriers is $\overline{K} = 60$. It is assumed that the number of uplink UE multipaths is 3 and the number of radar target paths is 1. The unified path delay τ_{l_a} is uniformly generated between 0 and 320 ns, and the maximum unified velocity $[v_{l_a}]_{max}$ is 30 m/s. The unified AoA θ_{l_a} and AoD ϕ_{l_a} are randomly sampled from $[-\frac{\pi}{2}, \frac{\pi}{2}]$, and the unified path gain γ_{l_a} is distributed to $\mathcal{CN}(0, 1)$. The signal-to-noise ratios (SNRs) $\frac{\|\mathcal{Y}-\mathcal{N}\|_F^2}{\|\mathcal{N}\|_F^2}$ are set from 0 dB to 20 dB. To characterize the accuracy of AUD, the active detection accuracy (ADA) is selected as the performance metric, given by

$$\mathrm{ADA}=\frac{[\hat{\mathbb{A}} \cap \mathbb{A}]_c}{[\mathbb{A}]_c}, \tag{31}$$

where $\hat{\mathbb{A}}$ and $\mathbb{A}$ are the estimated and true sets of active users, respectively. To characterize the estimation performance of the communication and sensing parameters, $\mathrm{NMSE}(\mathbf{H})$ and $\mathrm{NMSE}(\boldsymbol{x})$ are selected to evaluate the channel matrix estimation performance of active UEs and position estimation performance of radar targets, respectively, given by

$$\mathrm{NMSE}(\mathbf{H}) = \sum_{u} \sum_{k=1}^{K} \frac{\left\|\hat{\mathbf{H}}_u^k(N) - \mathbf{H}_u^k(N)\right\|_F^2}{\|\mathbf{H}_u^k(N)\|_F^2}, \tag{32}$$

$$\mathrm{NMSE}(\boldsymbol{x}) = \sum_{l_a=1}^{L} \frac{|\hat{\boldsymbol{x}}_{l_a} - \boldsymbol{x}_{l_a}|^2}{|\boldsymbol{x}_{l_a}|^2}. \tag{33}$$

Fig. 2 illustrates the ADA performance under various SNRs. It can be observed that the performance of the ALS-based algorithm increases slowly with the increase of SNR in the case of 5 active users and 5 radar targets. However, since

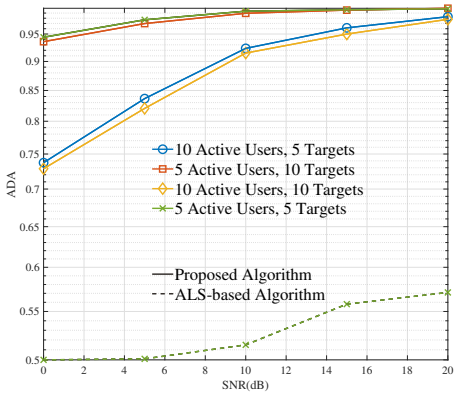

Fig. 2: ADA performance under various SNRs.

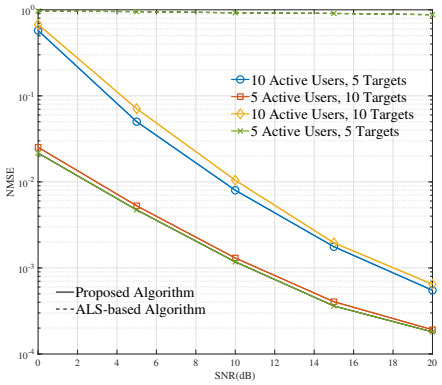

Fig. 3: Communication channel estimation performance under various SNRs.

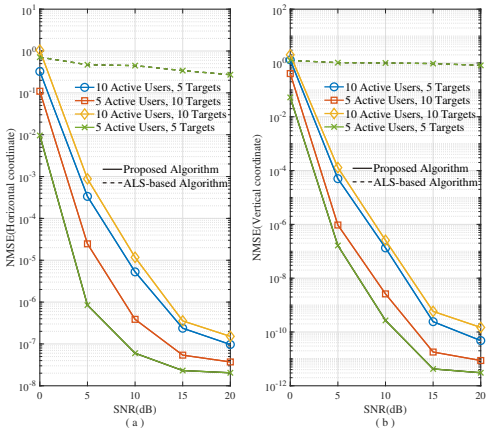

Fig. 4: Sensing position estimation performance under various SNRs.

the structure of the factor matrix is ignored by ALS-based algorithm, its performance is worse than our proposed algorithm. In contrast, our proposed algorithm maintains good performance regardless of the number of active users and radar targets. For instance, the ADA performance can reach 0.98 at SNR $= 20$ dB in the case of 10 active users and 5 radar targets, and 0.99 at SNR $= 10$ dB in the case of 5 active users and 10 radar targets, which verifies the effectiveness of our proposed algorithm on AUD. To be noticed, the performance of different algorithms are limited when the number of active users and targets are 10 and 10, respectively, due to the number of estimated path parameters increase significantly.

In Fig. 3, the communication channel estimation performance is presented. We can see that the communication channel estimation performance of the ALS-based algorithm has hardly improved with the increase of SNR, where the NMSE can only be around 10^0 when the SNR is 20 dB. In contrast, under the same situation of 5 active users and 5 radar targets, the NMSE of our proposed algorithm can reach nearly 10^{-4} when the SNR is 20 dB, which shows the superiority on communication parameter estimation.

Fig. 4 shows the sensing position estimation performance. Fig. 4(a) and Fig. 4(b) show the NMSE curves of the estimated targets on the horizontal and vertical axes, respectively. Obviously, the performance of the ALS-based algorithm does not improve significantly with the increase of SNR, while the performance of the proposed algorithm improves. Specifically, when SNR $= 10$ dB, in the case of 5 active users and 5 radar targets, the NMSE performance of the ALS-based algorithm on both the horizontal and vertical axes is around 10^0. In contrast, under the same situation, the NMSE performance of our proposed algorithm on the horizontal and vertical axes can reach 10^{-7} and 10^{-9}, respectively, which proves the reliability on radar sensing resolution.

VI. Conclusions

In this paper, the signal model of ISAC combined with the GF-RA system was first converted into a unified CPD-based form. Then, a matrix subspace-based method was proposed to accurately estimate the factor matrices where the communication and sensing parameters can be extracted. To tackle the issue of coupled parameters, an alternating iterative estimation algorithm was proposed. Simulation results demonstrated that our proposed joint communication and sensing parameter estimation algorithm based on CPD performs well under large-scale user access, which shows outstanding performance in AUD, channel estimation, and radar sensing.

References

[1] N. Wu et al., "AI-Enhanced integrated sensing and communications: Advancements, challenges, and prospects," *IEEE Commun. Mag.*, vol. 62, no. 9, pp. 144-150, Sep. 2024.

[2] Z. Zhou, J. Fang, L. Yang, H. Li, Z. Chen, and R. S. Blum, "Low-rank tensor decomposition-aided channel estimation for millimeter wave MIMO-OFDM systems," *IEEE J. Sel. Areas Commun.*, vol. 35, no. 7, pp. 1524–1538, Jul. 2017.

[3] R. Zhang et al., "Integrated sensing and communication with massive MIMO: A unified tensor approach for channel and target parameter estimation," *IEEE Trans. Wireless Commun.*, vol. 23, no. 8, pp. 8571–8587, Aug. 2024.

[4] R. Zhang, L. Cheng, S. Wang, Y. Lou, W. Wu, and D. W. K. Ng, "Tensor decomposition-based channel estimation for hybrid mmWave massive MIMO in high-mobility scenarios," *IEEE Trans. Commun.*, vol. 70, no. 9, pp. 6325–6340, Sep. 2022.

[5] B. Wang, L. Dai, Y. Zhang, T. Mir, and J. Li, "Dynamic compressive sensing-based multi-user detection for uplink grant-free NOMA," *IEEE Commun. Lett.*, vol. 20, no. 11, pp. 2320–2323, Nov. 2016.

[6] L. Liu and W. Yu, "Massive connectivity with massive MIMO—Part II: Achievable rate characterization," *IEEE Trans. Signal Process.*, vol. 66, no. 11, pp. 2947–2959, Jun. 2018.

[7] M. F. Keskin, H. Wymeersch, and V. Koivunen, "MIMO-OFDM joint radar-communications: Is ICI friend or foe?" *IEEE J. Sel. Topics Signal Process.*, vol. 15, no. 6, pp. 1393–1408, Nov. 2021.

[8] J. Wang, W. Zhang, Y. Chen, Z. Liu, J. Sun, and C.-X. Wang, "Time-varying channel estimation scheme for uplink MU-MIMO in 6G systems," *IEEE Trans. Veh. Technol.*, vol. 71, no. 11, pp. 11820–11831, Nov. 2022.

[9] G. Liu, A. Liu, R. Zhang, and M. Zhao, "Angular-domain selective channel tracking and Doppler compensation for high-mobility mmWave massive MIMO," *IEEE Trans. Wireless Commun.*, vol. 20, no. 5, pp. 2902–2916, May. 2021.

[10] L. Cheng, Y.-C. Wu, and H. V. Poor, "Probabilistic tensor canonical polyadic decomposition with orthogonal factors," *IEEE Trans. Signal Process.*, vol. 65, no. 3, pp. 663–676, Feb. 2017.

[11] M. Sørensen and L. De Lathauwer, "Blind signal separation via tensor decomposition with Vandermonde factor: Canonical polyadic decomposition," *IEEE Trans. Signal Process.*, vol. 61, no. 22, pp. 5507–5519, Nov. 2013.

[12] T. G. Kolda and B. W. Bader, "Tensor decompositions and applications," *SIAM Rev.*, vol. 51, no. 3, pp. 455–500, Sep. 2009.